Catalysis Science & Technology

# Conversion of CO2 on a Highly Active and Stable Cu/FeOx/CeO2 Catalyst: Tuning Catalytic Performance by Oxide-Oxide Interactions

| | |
|---|---|
| Journal: | *Catalysis Science & Technology* |
| Manuscript ID | CY-ART-04-2019-000722.R1 |
| Article Type: | Paper |
| Date Submitted by the Author: | 21-May-2019 |
| Complete List of Authors: | Lin, Lili; Brookhaven National Laboratory, Chemistry Department<br>Yao, Siyu; Brookhaven National Laboratory, Chemistry Department<br>Rui, Ning; Brookhaven National Laboratory, Department of Chemistry<br>Han, Lili; University of California Irvine, Department of Physics<br>Zhang, Feng; SUNY Stony Brook, Materials Science & Enginerring<br>Gerlak, Clifford; Brookhaven National Laboratory, Chemistry Department<br>Liu, Zongyuan; Brookhaven National Laboratory, Chemistry Department<br>cen, Jiajie; Stony Brook University<br>Song, Lian; SUNY Stony Brook, Materials Science & Engineering<br>Senanayake, Sanjaya; Brookhaven National Laboratory, Chemistry<br>Xin, Huolin; University of California Irvine, Department of Physics<br>Chen, Jingguang; Columbia University, Chemical Engineering<br>Rodriguez, Jose; Brookhaven National Laboratory, Chemistry Department |
| | |

ARTICLE

# Conversion of $CO_2$ on a Highly Active and Stable Cu/FeOx/$CeO_2$ Catalyst: Tuning Catalytic Performance by Oxide-Oxide Interactions

Received 00th January 20xx,

Accepted 00th January 20xx

DOI: 10.1039/x0xx00000x

Lili Lin[a], Siyu Yao[a], Ning Rui[a], Lili Han[b], Feng Zhang[c], Clifford Gerlak[a], Zongyuan Liu[a], Jiajie Cen[c], liang Song[c], Sanjaya Senanayake[a], Huolin L. Xin[b], Jingguang G. Chen[a], José A. Rodriguez*[acd]

Nanoparticles of $FeO_x$ dispersed on ceria exhibit unique chemical and textural properties. They undergo a dynamic $FeO_x \leftrightarrow Fe$ transformation depending on the reaction conditions. The high density Fe oxide clusters dispersed over $CeO_2$ are effective texture promoters that enhance the stability of $Cu/CeO_2$ catalyst in the high temperature reverse water gas shift reaction. At the optimal Fe loading, the deactivation rate constant of a $5Cu1.6Fe/CeO_2$ catalyst is only 0.003 $h^{-1}$, five times smaller than that of the monometallic $5Cu/CeO_2$ catalyst. In-situ XRD, AP-XPS and XAFS characterizations reveal that the partially reduced Fe nanoparticles would be oxidized by $CO_2$ in the reductive atmosphere and re-disperse into high density $FeO_x$ clusters under the high temperature $CO_2$ hydrogenation process. The wetting phenomenon, maximizing the density of $FeO_x$ particles on the $CeO_2$ support, benefits from strong oxide-oxide (Fe-O-Ce) interactions.

## Introduction

In heterogeneous catalysis, studies of solid-solid wetting are essential for the preparation of effective catalysts. [1-3] Many metal-oxide interfaces are characterized by weak interactions between their components leading to poor dispersion and sintering of the metal particles. Transition metal oxides exhibit higher tendency to disperse over oxide supports when compared to metallic particles due to the similar surface energy of the oxide compounds.[1-4] Using these interfacial properties, it has been demonstrated to be possible and effective to enhance the dispersion of loaded metal species, develop isolated high valence metal oxides[5] and regenerate sintered metal particles in a flow of $O_2$ at elevated temperature[6, 7]. When analyzing the chemical bonding of oxide-oxide interfaces at atomic scale, the 'metal-O-metal' linkage is a key structural unit that can involve strong bonding interactions which can lead to unique chemical and textural properties.[8] Therefore, the introduction of a high density oxide compound as a texture promoter that may be able to isolate finely dispersed metal particles, in particular under working condition, is a potentially effective solution to enhance the high temperature stability of traditional metal/oxide systems.

Copper/ceria catalysts have been extensively studied for the reverse water gas shift (RWGS, $CO_2 + H_2 \rightarrow CO + H_2O$), a high temperature favorable reaction for carbon dioxide utilization[9, 10], due to their excellent catalytic performance and low cost [11-13]. However, $Cu/CeO_2$ catalysts are not suitable for high temperature operation because of strong sintering causes a loss of active Cu sites and deactivation under working condition[14]. To prevent the surface migration of Cu, a texture promoter should bind well with both the admetal and ceria support. Furthermore, as the RWGS reaction generally occurs under $H_2$-rich condition, the oxides should not be de-wetting under a $H_2$-rich atmosphere. Otherwise, the steric hindering effect of the promotor would be lost. Doping the ceria lattice with some elements (Zr, Tb, Gd, Sm, etc) could change the morphological and structural properties of the oxide enhancing its ability to bind metals.[2] Dopants such as Gd and Sm can be involved with defect formation trapping admetals.[2] Here, we have followed a different approach. In previous studies, it has been found that $FeO_x$ species could form strong bonds with $CeO_2$[15, 16]. Benefiting from the high oxygen mobility of $CeO_2$ and the strong bonding interactions, Fe remained in the form of oxide particles and did not severely aggregate in redox cycles at 600-800 °C[17]. As a result, highly dispersed $FeO_x$ species might be a potential texture promoter for the high temperature RWGS reaction. Furthermore, $FeO_x$ particles bound to ceria could have special chemical and catalytic properties as a consequence of their small size and the Fe-O-Ce linkage.

[a] Chemistry Department, Brookhaven National Laboratory, Upton, New York 11973, United States.
[b] Department of Physics and Astronomy, University of California, Irvine, CA 92697, USA.
[c] Materials Science and Chemical Engineering Department, State University of New York at Stony Brook, New York, 11794, United States
[d] Department of Chemistry, State University of New York at Stony Brook, New York 11794, United States.
*Corresponding author: rodriguz@bnl.gov

Electronic Supplementary Information (ESI) available: BET surface area, EXAFS fitting results. See DOI: 10.1039/x0xx00000x

In this paper, we will use in-situ measurements to show that nanoparticles of iron oxide undergo a dynamic $FeO_x \leftrightarrow Fe$ transformation when cycling between oxidizing and reducing reaction conditions. $FeO_x$ is a highly effective and stable texture promoter for the $Cu/CeO_2$ catalysts under high temperature RWGS reaction conditions. For an optimal loading, the $5Cu1.6Fe/CeO_2$ catalyst exhibits significantly improved stability without the sacrifice of $CO_2$ hydrogenation activity. In a 45-hr stability tests, the deactivation rate constant of the $5Cu1.6Fe/CeO_2$ catalyst is only 0.003 $h^{-1}$ much smaller than that of the monometallic $5Cu/CeO_2$ catalyst (0.014 $h^{-1}$). The in-situ XRD, XAFS and AP-XPS characterizations demonstrate that Fe species form highly dispersed $FeO_x$ clusters over the $CeO_2$ support. Even when the Fe is fully reduced into metallic particles, they can still be oxidized by the $CO_2$ in the gas feed and re-disperse into fine $FeO_x$ clusters spontaneously under the influence of Fe-O-Ce interactions.

## Experimental Methods

### Catalysts Synthesis

The $5Cu/CeO_2$, $5CuxFe/CeO_2$ and $xFe/CeO_2$ systems (the 5 or x mean the weight percentage of loaded metals) were synthesized using a deposition impregnation (DP) method over commercial $CeO_2$ supports (Sigma-Aldrich, < 25 nm)[18, 19]. In a typical synthesis process, the $CeO_2$ supports were dispersed in deionized water under vigorous stirring. The aqueous solution with the desired metals precursor composition and concentration was added into the suspension drop by drop. The pH of the suspension was tuned at 9.0 by a sodium carbonate solution. After all the precursor solution was added, the suspension was further stirred for another 2 hrs, then aged for 2 hrs. The suspension was filtered and the filtrate was washed by deionized water six times, and dried at 60 and 120 °C for 6 hrs sequentially. The dried samples were further calcined to 650 °C with a heating rate of 10 °C/min and hold at 650 °C for 4 hrs. The loadings of Cu and Fe in the catalysts were determined by ICP-OES.

### Performance Evaluation

The catalytic performances of the as-synthesized catalysts in the RWGS reaction were evaluated in a fixed-bed reactor at atmospheric pressure. Under a typical experiment, ~10 mg of catalyst were mixed with 10 mg of $SiO_2$ (40-60 mesh, calcined at 900 °C for 4 hrs before use) and loaded into a quartz tube (1/4 inch diameter). Before reaction, the catalyst was reduced in a mixture of 50%$H_2$ in $N_2$ at 500 °C for 2 h. For the $Cu/CeO_2$ catalyst, the reduction temperature was set at 400 °C. After reduction, the temperature was raised to the reaction temperature of 600 °C at a ramp rate of 10 °C/min in the stream of $N_2$, then held it at 600 °C in the reactant gas (30ml/min $CO_2$, 30ml/min $H_2$ and 40 ml/min $N_2$) for stability tests. The $N_2$ in the gas flow was both the inner standard and carrier gas. In order to prevent the condensation of water, the outlet pipe was wrapped with heating tapes kept at 110 °C. The composition of the products was analyzed by an on-line gas chromatography (GC, Agilent 7890) equipped with a thermal conductive detector (TCD) and a flammable ionization detector (FID).

The conversion and selectivity of the reaction was defined as:

$$\text{Conv.}(CO_2) = (F(CO_2)_{inlet} - F(CO_2)_{outlet})/\text{F}(CO_2)_{inlet}$$

$$\text{Sel.}(\text{CO}) = F(CO)_{outlet}/(F(CH_4)_{outlet} + F(CO)_{outlet})$$

The deactivation rate ($k_d$)[6, 20] was calculated based on the 40 hr stability test, its definition being:

$$k_d = \frac{1}{t}(ln\frac{1 - Conv.(CO_2)_t}{Conv.(CO_2)_t} - ln\frac{1 - Conv.(CO_2)_0}{Conv.(CO_2)_0})$$

This model presumes that the deactivation follows a first order kinetics. $Conv.(CO_2)_t$ means the conversion of the $CO_2$ at the time of t, while the $Conv.(CO_2)_0$ means the initial conversion of the $CO_2$, higher $k_d$ values being indicative of rapid deactivation, that is, low stability.

### Structure Characterization

#### In-situ X-ray diffraction (XRD)

In-situ XRD measurements were performed at the 17-BM station of the Advanced Photon Source (APS) at Argonne National Laboratory (ANL) and the 28-ID station of the National Synchrotron Light Source II (NSLS-II). The in-situ setup was described in a previous work in detail[21-23]. About 5 mg of catalyst were loaded into an amorphous silica capillary with 0.9 mm inner diameter. The scan rate was around 1 min per spectrum. The protocol for in-situ XRD was as follows, (1) reduce the sample at a given temperature for reaction studies with a ramping rate of 10 °C/min, holding at the final temperature for 30 min. (2) increase the temperature to a reaction temperature of 600 °C, and hold at for 1 h in the presence of the reactant gas ($CO_2/H_2$=1:1). Two-dimensional XRD images were continuously collected by a PerkinElmer flat panel detector. The images were subsequently processed with GSAS-II to obtain XRD profiles, and Rietveld refinement was performed to extract phase and other structural information.

#### Ambient Pressure X-ray Photo Spectroscopy

A commercial SPECS AP-XPS chamber equipped with a PHOIBOS 150 EP MCD-9 analyzer at the Chemistry Division of BNL was used for XPS analysis (energy resolution: ~ 0.5 eV). The Ce 3*d* photoemission line with the strongest $Ce^{4+}$ feature (916.9 eV) was used for the energy calibration[21]. The catalyst powder was pressed on an aluminum plate and then loaded into the AP-XPS chamber. The sample was pre-treated by heating it in 30 mTorr of $H_2$ at 500 °C for 60 min. After cooling down to room temperature, 30 mTorr of $H_2$ and 30 mTorr of $CO_2$ were introduced into the reaction chamber through a high precision leak valve. Under the reaction conditions, the temperature was raised to 250, 350, 450 and 500 °C. Before collecting data, each temperature was held for 30 min to reach a steady state surface composition. The Ce 3*d*, Cu 2*p*, Cu LMM, O 1*s*, and C 1*s* XPS regions[24] were collected at 25 °C for a fresh sample, after reduction at 500 °C, and at different temperatures (25, 250, 350, 450 and 500 °C) under the simulated reaction gas environment. The spectrum of the fresh sample was collected under UHV

conditions. The data were analyzed by using CasaXPS software. The surface atomic ratio of a given element is defined as:

$$\frac{\mathrm{M}}{\mathrm{N}} = (\mathrm{A}_M * RSF_M)/(\mathrm{A}_N * RSF_N)$$

Where $A_M$ is the peak area measured at a particular radiation of M and RSF is the response factor at that radiation, which is obtained from reference[25]. The RSFs of Cu, Fe and Ce were chosen as Cu 2*p* 3/2, Fe 2*p* 3/2 Ce 3*d*.

**In-situ X-ray absorption fine structure (XAFS) spectroscopy**

The in-situ XAFS spectra of Cu and Fe were collected at the 9-BM station of the Advanced Photon Source (APS) at Argonne National Laboratory (ANL). The flow cell setup was home designed as shown in references[15, 26]. Approximately 50 mg of catalyst were loaded in the micro-channel of the reactor with graphite paper sealed as the window material. The fluorescence spectra were collected using a vortex detector. The samples were first reduced in a gas mixture of 50%$H_2$/$N_2$ for 30 min. Then heated to the reaction temperature of 600 °C at a rate of 10 °C/min, and switching the gas to the reactant gas ($CO_2$/$H_2$:He=1:1:1) for 60 min. The spectra (three scans for each) were collected under in-situ conditions and then analyzed using the IFEFFIT package[27]. Cu foil, CuO, $Cu(OH)_2$, Fe foil, FeO, $Fe_3O_4$, and $Fe_2O_3$ were employed as references for EXAFS fitting.

**STEM-EDX elemental mapping**

The TEM samples were prepared by dropping the sample suspension onto molybdenum grids coated with carbon film. HAADF-STEM images and EDS mappings were obtained using a FEI Talos F200X S/TEM microscope with a field-emission gun at 200 kV. The specific element mapping of Fe was obtained using Fe $K_\beta$ (7.060 keV) radiation to prevent the overlap of Fe and Ce.

## Results and discussions

**Stability evaluation of $Cu/CeO_2$ and $CuFe/CeO_2$ catalysts for the RWGS at 600 °C**

The performance of a standard copper-ceria catalyst was evaluated. The Cu based catalysts generally showed excellent $CO_2$ hydrogenation activities, but tended to deactivate quickly at 600 °C in the RWGS atmosphere. As shown in Figure 1A, both $Cu/CeO_2$ and a commercial $Cu\text{-}ZnO/Al_2O_3$ catalyst (Alfa Aesar) deactivate quickly at 600 °C, due to the sintering of the highly dispersed Cu centers. Even by using $CeO_2$, a reducible oxide support that is able to anchor metal centers using strong metal support interaction[28], the $Cu/CeO_2$ catalyst still losses about 35% of its activity in 40 hrs. Therefore, promoters are necessary to enhance the stability of Cu based catalysts in the high temperature reverse water gas shift reaction.

FeOx nanoparticles were used to help anchor Cu on ceria. The plain $FeO_x/CeO_2$ did show catalytic activity by itself, Figure 1A, exhibiting a performance which was comparable or better than that of a commercial $Cu\text{-}ZnO/Al_2O_3$ catalyst. The stabilizing effect of the $FeO_x$ promoter on the $Cu/CeO_2$ catalyst was evaluated using a series of 5CuxFe/$CeO_2$-DP catalysts (where x represents the desired loading of Fe, weight percentage)[18, 19]. The ICP-OES (see Table S1) results suggest that all the catalysts had the designated loading of Cu and Fe. The BET measurements showed that the mass specific surface area of all the catalysts was around 40 $m^2$/g (Table S1). The catalytic performances of the as-synthesized $CuFe/CeO_2$ catalysts was also evaluated under the RWGS reaction at 600 °C for 40 hrs (Figure 1B and C). The introduction of the Fe promoter led to significant improvement on the stability of the $Cu/CeO_2$. When the iron loading was 0.8%, the deactivation rate constant ($k_d$), a quantification of the deactivation rate (assuming the deactivation obey 1st order kinetics), decreased from 0.014 to 0.010 $h^{-1}$. At 1.6% Fe loading, the $CO_2$ conversion becomes relatively stable after a short induction period and the $k_d$ further decreased to only 0.003 $h^{-1}$. Interestingly, a further increment of the Fe loading causes a drop of the stability of the $CuFe/CeO_2$ catalyst. Thus, the 5Cu1.6Fe/$CeO_2$ is the optimal ratio to improve the stability. To understand what kind of function the Fe promoters perform in the $CuFe/CeO_2$ catalysts and the reason for the optimal Fe loading for stability enhancement, a serial of detailed structural characterizations was performed on the working catalysts.

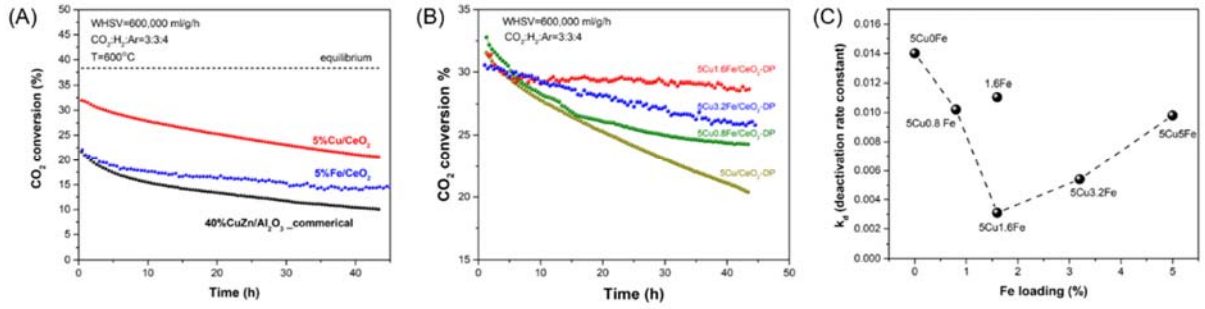


**Figure 1. The performance and stability evaluation of a series of $CuFe/CeO_2$ catalysts.** The RWGS activity and stability tests of **(A)** 5% $Cu/CeO_2$ and 40%$CuZn/Al_2O_3$-commercial catalysts and **(B)** 5%$Cu/CeO_2$ catalysts modified with different loadings of iron promoters (0.8, 1.6 and 3.2 wt%), and 1.6$Fe/CeO_2$ catalyst, **(C)** the relationship between deactivation rate constant ($k_d$) and iron loadings of the $CuFe/CeO_2$ catalysts. The calculation of $k_d$ was based on the stability test shown in Figure 1B. The reaction conditions are $CO_2$: $H_2$:$N_2$=3:3:4 with a weight hour space velocity of 600,000 ml/g/h.

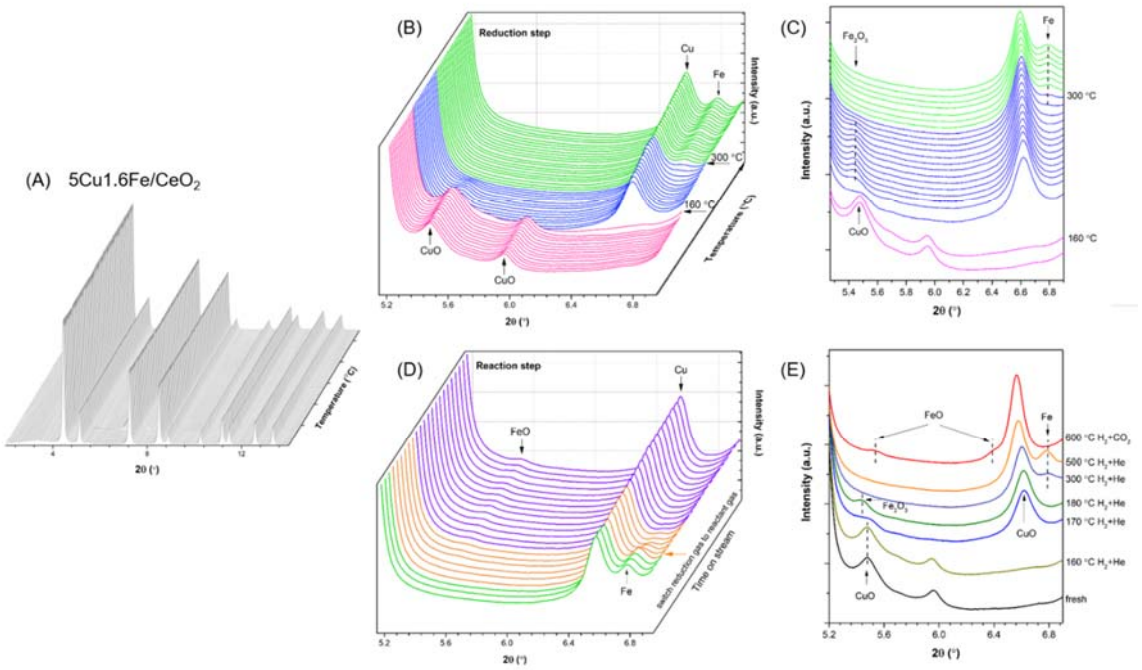


**Figure 2. Evolution of in-situ XRD profiles for 5Cu1.6Fe/$CeO_2$ catalyst under various reaction conditions. (A)** The whole range for in-situ XRD profiles covering reduction and reaction condition. **(B)** and **(C)** profiles in the 2θ range of 5.15-6.9° during the reduction process (50%$H_2$/He). **(D)** Profiles in the 2θ range of 5.15-6.9° under $CO_2$ hydrogenation conditions ($CO_2$:$H_2$=1:1). **(E)** Profiles in the 2θ range of 5.15-6.9° from reduction conditions to reaction conditions.

**In-situ structural characterizations**

The crystal structural evolution of the 5Cu1.6Fe/$CeO_2$ catalyst was monitored by time-resolved in-situ X-ray diffraction (XRD) under both reduction and reaction conditions. As shown in Figure 2A, no significant crystal structure change has been found for the ceria support. As a result, we focused on the redox properties of the loaded Cu and Fe species. The assignment of major diffraction peaks and related crystal phases was listed in Table S2. Besides ceria, the only observable crystal phase in the fresh sample was CuO. The absence of Fe oxides diffraction peaks suggests that these species were finely dispersed beyond the detection limit of the XRD method. Based on the in-situ XRD characterization, most of the CuO is reduced to metallic Cu at 160 ~170 °C by hydrogen (Figure 2B and C, magenta line). Simultaneously, a small feature around 5.44° appears, which is assigned to $Fe_2O_3$ [15]. This phenomenon is associated with the phase separation of the highly dispersed $CuFe_2O_4$ after the reduction of Cu (II)[29]. When the reduction temperature reaches 300 °C, the metallic Fe (green line) diffraction peak centered at 6.79° appeared. After holding at 500 °C for an hour under reduction condition, the sample is further heated to 600 ° in $N_2$ atmosphere, and then exposes to the reaction gases. As soon as the atmosphere changes to a $CO_2$/$H_2$ reactant gas, the diffraction peaks of metallic Fe disappear rapidly and a broad weak feature of FeO shows up at 6.38° (Figure 2D, E and Table S2), indicating that the Fe NPs transform into smaller oxide particles in the $CO_2$ and $H_2$ mixture. This oxidative wetting phenomenon is probably due to the strong interaction between $FeO_x$ and $CeO_2$ and the similar surface energy of $FeO_x$ and $CeO_2$ support[30-32]. Meanwhile, the bulk phase of metallic Cu on $CeO_2$ remains intact at 600 °C [21]. Therefore, the metallic Cu and Fe oxides on $CeO_2$ are probably the active phase for the RWGS reaction. The re-dispersion of Fe species can occur to any Fe loadings (0.8, 2.4 and 3.2%). However, at high Fe loading of 3.2%, the

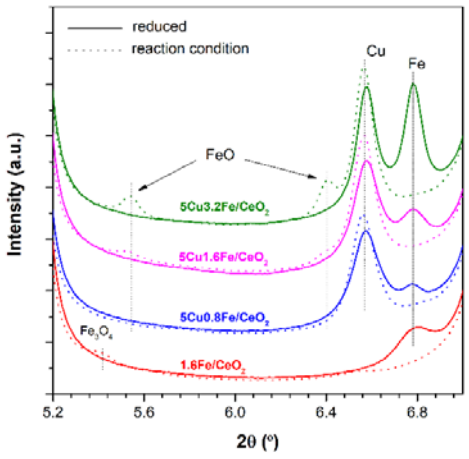


**Figure 3.** The XRD profile of 5CuxFe/$CeO_2$ and 1.6Fe/$CeO_2$ catalysts under reduction (dash line) and reaction (solid line) conditions. The reduction and reaction conditions are the same listed in the caption of Figure 2.

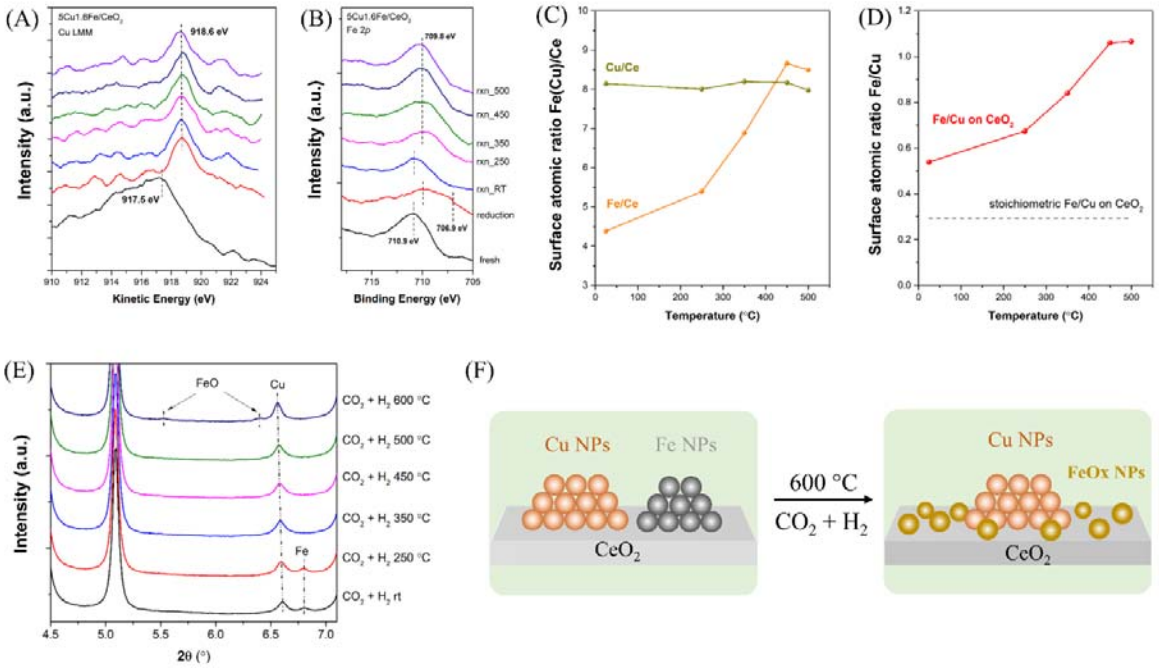


**Figure 4. Structure characterization of 5Cu1.6Fe/$CeO_2$ catalysts. (A)** Cu LMM, **(B)** Fe 2*p* profiles of 5Cu1.6Fe/$CeO_2$ catalysts under different reaction conditions; **(C)** surface ratio of Fe/Ce and Cu/Ce analyzed by XPS from room temperature to 500 °C under reaction conditions. **(D)** surface ratio of Fe/Cu compared with stoichiometric ratio Fe/Cu on $CeO_2$. The stoichiometric of 5Cu1.6Fe/$CeO_2$ catalyst was measured by ICP-OES, which was determined to be 5.4wt% Cu and 1.56 wt% Fe in the catalyst. **(E)** The crystal phase evolution of the supported Cu and Fe species of 5Cu1.6Fe/$CeO_2$ under stepwise heating after reductions. **(F)** Illustration of thermally induced Fe nanoparticle re-dispersion and preventing Cu nanoparticles from aggregation under oxidative hydrogenation atmosphere (v($CO_2$) : v($H_2$) =1:1) at high temperature of 600 °C.

diffraction peaks of FeO get much stronger even after re-dispersion (Figure 3), suggesting that the average dimension of FeO particles become larger may because of the limited BET surface area. This might be related with the less efficiency of Fe promoters in the 5Cu3.2Fe/$CeO_2$ RWGS catalyst. Therefore, it could be inferred that keeping the high density of Fe clusters as textural promoters under the high temperature RWGS condition and preventing the formation of large FeO particles are very important to enhance the stability of Cu/$CeO_2$ catalysts.

AP-XPS measurements were performed on the 5Cu1.6Fe/$CeO_2$ catalyst to examine the oxidation state and surface concentration of the surface elements at elevated temperature under different atmospheres. After $H_2$ reduction, the Cu LMM K.E. peak shifted to 918.6 eV, indicating the Cu species are fully reduced to metallic copper[24, 33]. Even after the reaction gas is introduced, no shift of the Auger electron peak occurs, suggesting that surface Cu (0) tends not to be oxidized by $CO_2$ in the $CO_2$:$H_2$=1:1 atmosphere (Figure 4A), further confirming that $Cu^0$ on the $CeO_2$ support is the active phase for the RWGS reaction[21]. The Fe 2*p* region XPS profiles of the reduced sample demonstrate the Fe species loaded on the catalysts were a mixture of Fe(0) and Fe oxides, which could be seen from the binding energy of Fe located at 706.9 and 709.8 eV[24, 34]. When compared with the in-situ XRD results, it suggests that there was still a large amount of unreduced $FeO_x$ clusters dispersed on the $CeO_2$ support after hydrogen reduction. When the atmosphere was switched to a $CO_2$-$H_2$ mixture, an immediate heal of the oxygen vacancies of the ceria support (Figure S1) and a simultaneous re-oxidation of the Fe to Fe(III) occurred at room temperature (Figure 4B). When heating the sample in the $CO_2$ and $H_2$ mixture, the reduction of $CeO_2$ support and the partial reduction from Fe(III) to $FeO_x$ (the valence of Fe is between II~III, as the B.E. of Fe shift from 710.9 eV to 709.8 eV[17]) occurred on the Cu5Fe1.6/$CeO_2$ catalyst at above 250 °C. We further calculated the surface ratio of Fe/Ce and Cu/Ce to confirm the existence of the oxidation induced re-dispersion phenomenon. As shown in Figure 4C, the surface atomic ratio [17, 25] of Cu/Ce keeps constant around 8 under all conditions, indicating the size of Cu domains was relatively stable at elevated temperature. In contrast, the ratio of Fe/Ce was only 4 at room temperature. With the increasing temperature, the ratio of surface Fe/Ce increased significantly to over 8.5. The final ratio of Fe and Cu on the surface reaches over 1:1 (Figure 4D), which is much larger than the stoichiometric value 0.33 ($mol_{Fe}$=1.56/56 $mol_{Cu}$=5.6/64), demonstrating that the Fe oxide domains were smaller than the Cu particles and more Fe was exposed on the surface. The AP-XPS results at different reaction temperature show that the $FeO_x$ species would be wetting on the $CeO_2$ surface at elevated temperature in the $CO_2$+$H_2$ mixture, which implies that a high dispersion of $FeO_x$ on $CeO_2$ is thermodynamically more favorable. Due to the wetting phenomenon, the density of $FeO_x$ would be maximized on the support, providing a positive stabilizing effect to immobilize Cu particles and prevent inter particle aggregation (Figure 4E and F).

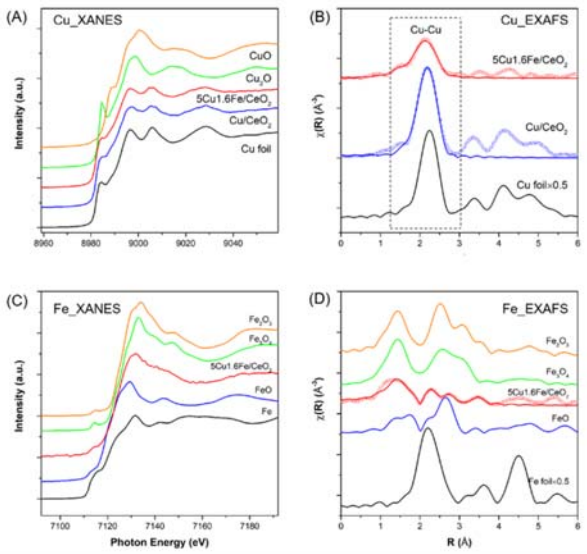


**Figure 5. In-situ XAFS characterization of 5Cu1.6Fe/$CeO_2$ and 5Cu/$CeO_2$ catalysts. (A)** XANES and **(B)** EXAFS fitting results for the Cu K edge of 5Cu1.6Fe/$CeO_2$ and 5Cu/$CeO_2$ catalysts under reaction conditions ($CO_2$:$H_2$=1:1) at 600 °C; **(C)** XANES and **(D)** EXAFS fitting results of K edge of 5Cu1.6Fe/$CeO_2$ catalyst.

The dispersion and average size of metallic Cu and $FeO_x$ in the 5Cu1.6Fe/$CeO_2$ catalyst were then determined by in-situ XAFS characterization to further elucidate the role of Fe promoter. Based on the Cu K edge XANES spectra (Figure 5A), Cu species in the 5Cu1.6Fe/$CeO_2$ keep metallic state under reaction condition, which goes well with the XRD and AP-XPS characterizations. The corresponding coordination number of metallic Cu-Cu from EXAFS fitting results is determined to be 5.3 (Figure 5B and Table S3), indicating that the average particle size of Cu NPs on 5Cu1.6Fe/$CeO_2$ was ca. 1 nm based on the half sphere model [35]. Compared with the monometallic Cu/$CeO_2$ reference catalyst with similar Cu loading (the average coordination number of Cu-Cu is 9.0), the average particle size of Cu(0) decreases significantly, demonstrating that the promotion effect of Fe had effectively limited the size of Cu particles on $CeO_2$ at high temperature. The structure of Fe was further revealed by the Fe K edge XAFS method. The XANES spectrum (Figure 5C and Table S4) showed that the average oxidation state of Fe in the catalyst was between Fe(II) and Fe(III), suggesting that there were amorphous Fe(III) oxide species dispersed on $CeO_2$ besides the XRD-visible FeO crystallites. The EXAFS spectrum of Fe under reaction conditions shows that the C.N. of Fe-O (3.2) to C.N. of Fe-(O)-Fe ratio (1.6) was relatively much bigger than Fe oxide references, indicating that the Fe oxide species were highly dispersed over the $CeO_2$ support with a limited dimension (Figure 5D). Meanwhile, it is also proven that the ultra-small Fe particles were in close contact with the $CeO_2$ support, as the existence of Fe-Ce coordination shell near 3.8 Å is confirmed by EXAFS fitting (Table S5 and Figure S3). This interaction implies that the $FeO_x$ clusters were immobilized tightly on the ceria support.

## Discussion

It is remarkable that $FeO_x/CeO_2$, without Cu or other admetal, is able to catalyze the hydrogenation of $CO_2$ while typical oxide supports such as $CeO_2$ or ZnO do not have catalytic activity. One can imagine a reduction (reaction with $H_2$) and oxidation process (activation and decomposition of $CO_2$) on the Fe centers that establishes a catalytic cycle and the $FeO_x/CeO_2$ systems has a performance comparable or better than that of a better than that of a commercial Cu-ZnO/$Al_2O_3$ catalyst. In previous studies it has been reported that catalysts containing the pair $FeO_x/CeO_2$ as a support are active for CO oxidation and the water-gas shift reaction.[37-39] Evidence for a Ce-Fe synergism was found in a Au/$CeO_2$-$FeO_x$/$Al_2O_3$ catalysts for $H_2$ production through the water-gas shift process.[39] Assuming that the RWGS goes through a OCOH intermediate,[37-39] the formation of OH bonds with the $FeO_x$ groups present in the surface could facilitate the evolution of CO gas.

Combining all the characterization results, it is clear that the FeOx species are very efficient as texture promoters in the Cu-Fe/$CeO_2$ bimetallic catalysts and the high density of Fe oxide (II and III) clusters dispersed over the $CeO_2$ support do not reduce under a hydrogen rich reaction atmosphere. The function of the $FeO_x$ clusters as texture modifiers largely benefits from the high oxygen mobility in the $CeO_2$ support[36] and the strong oxygen affinity of Fe. These properties enable the $CeO_2$ support and Fe species to extract oxygen from the partial dissociation of the $CO_2$ molecule keeping Fe in a high valence state instead of being reduced and further aggregating into large metallic particles.

To further understand the important role of $FeO_x$, we evaluated the stability of the 5Cu1.6Fe/$CeO_2$ catalyst without pre-reduction (Figure 6), inferring from the above results that the Cu will be reduced to metallic as active sites and the $FeO_x$ species will still keep a good dispersion of the same state after calcination in the $CO_2$+$H_2$ reaction atmosphere (also confirmed by the in-situ XRD characterization as shown in Figure S4). As the images of as-synthesized 5Cu1.6Fe/$CeO_2$ catalyst shown in the Figure 6A, the Cu is well dispersed on the $CeO_2$, with Fe

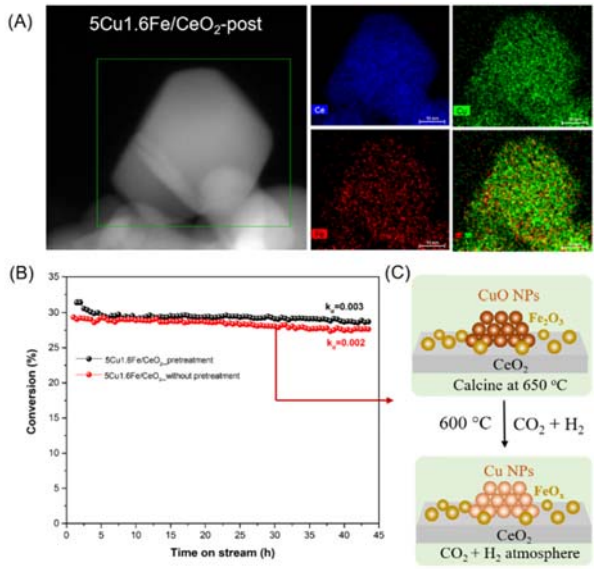


**Figure 6. Structure characterization and performance evaluation of fresh 5Cu1.6Fe/$CeO_2$. (A)** HAADF-STEM and elemental mapping images of post samples of 5Cu1.6Fe/$CeO_2$ catalyst. The elemental mappings of Ce, Cu and Fe are marked in blue, green and red, respectively. **(B)** The RWGS activity and stability comparison of 5Cu1.5Fe/$CeO_2$ with and without pre-treatment. **(C)** Illustration of the structure evolution of 5Cu1.6Fe/$CeO_2$-fresh in the reaction condition ($CO_2$ : $H_2$=1:1).

species acting as a structural promotor among the Cu NPs. Then, it could be seen from Figure 6B that no induction period appears at the beginning 3 hrs and a similar stability compared to the pre-treatment catalyst is achieved. This phenomenon demonstrates that the existence of fine dispersed Fe oxide clusters has identical ability with the ones underwent re-dispersion processes in stabilizing Cu particles (Figure 6C). Therefore, it could be confirmed that the fine Fe oxide particles are effective texture promoters for Cu/$CeO_2$ catalysts in the RWGS reaction. Our approach is different from others in which elements such as Gd or Sm are added to the ceria lattice to enhance the binding of metals,[2] but a combination of the two approaches could yield good benefits.

## Conclusions

In summary, we have shown the importance of oxide-oxide interactions when developing catalysts for $CO_2$ hydrogenation. A $FeO_x$/$CeO_2$ mixed oxide system displays good catalytic activity. Furthermore, we have developed a Cu-Fe/$CeO_2$ catalyst which exhibits significantly enhanced stability when compared to mono-component Cu/$CeO_2$ catalysts for the RWGS reaction at high temperature. Detailed characterization results have shown that the active species in the Cu-Fe/$CeO_2$ systems are metallic Cu particles and highly dispersed $FeO_x$ oxide clusters. We have demonstrated that $FeO_x$ performs as a texture promoter to prevent the inter-particle aggregation of Cu(0) species. Under the RWGS condition at high temperature, the wetting phenomenon of the $FeO_x$ clusters on $CeO_2$ would maximize the density of the promoter. At the optimal condition, the 5Cu1.6Fe/$CeO_2$ catalyst shows the best stability and exhibits a much smaller deactivation rate constant (one order smaller) than a 5Cu/$CeO_2$ catalyst.

## Conflicts of interest

There are no conflicts to declare.

## Acknowledgements

The work carried out at Brookhaven National Laboratory was supported by the U.S. Department of Energy under contract no. DE-SC0012704. This research used resources 28-ID (XRD) beamline of the National Synchrotron Light Source II, a U.S. Department of Energy (DOE) Office of Science User Facility operated for the DOE Office of Science by Brookhaven National Laboratory under Contract No. DE-SC0012704. The in-situ experiments of this research used resources of the Advanced Photon Source (Beamlines 9BM (XAFS)and 17BM (XRD) at Argonne National Laboratory, which is a DOE Office of Science User Facility under contract no. DE-AC02- 06CH11357. This research also used resources of the Center for Functional Nanomaterials, specifically the electron microscopy facilities which is a U.S. DOE Office of Science Facility, at Brookhaven National Laboratory under Contract No. DE-SC0012704.

## Notes and references

1. Z. Liu, H. Zhang and Z. Chen, Applied Surface Science, 2014, 293, 326-331.
2. N.W. Kwak, S.J. Jeong, H.G. Seo, S. Lee, Y. Kim, J.K. Kim, P. Byeon, S.-Y. Cheung and W.C. Jung, Nature Communications, 2018, 9, 4829-4837.
3. J. A. Moulijn, A. Van Diepen and F. Kapteijn, Applied Catalysis A: General, 2001, 212, 3-16.
4. Y. Nagai, T. Hirabayashi, K. Dohmae, N. Takagi, T. Minami, H. Shinjoh and S. i. Matsumoto, Journal of Catalysis, 2006, 242, 103-109.
5. A. Aitbekova, L. Wu, C. J. Wrasman, A. Boubnov, A. S. Hoffman, E. D. Goodman, S. R. Bare and M. Cargnello, Journal of the American Chemical Society, 2018, 140, 13736-13745.
6. J. J. Sattler, J. Ruiz-Martinez, E. Santillan-Jimenez and B. M. Weckhuysen, Chemical reviews, 2014, 114, 10613-10653.
7. A. Iglesias-Juez, A. M. Beale, K. Maaijen, T. C. Weng, P. Glatzel and B. M. Weckhuysen, Journal of Catalysis, 2010, 276, 268-279.
8. R. Lang, W. Xi, J.-C. Liu, Y.-T. Cui, T. Li, A. F. Lee, F. Chen, Y. Chen, L. Li and L. Li, Nature communications, 2019, 10, 234.
9. O.-S. Joo, K.-D. Jung, I. Moon, A. Y. Rozovskii, G. I. Lin, S.-H. Han and S.-J. Uhm, Industrial & engineering chemistry research, 1999, 38, 1808-1812.
10. S. Saeidi, N. A. S. Amin and M. R. Rahimpour, Journal of CO2 utilization, 2014, 5, 66-81.
11. A. Tsai and M. Yoshimura, Applied Catalysis A: General, 2001, 214, 237-241.
12. C.-S. Chen, W.-H. Cheng and S.-S. Lin, Applied Catalysis A: General, 2003, 238, 55-67.

13. X. Zhang, X. Zhu, L. Lin, S. Yao, M. Zhang, X. Liu, X. Wang, Y.-W. Li, C. Shi and D. Ma, ACS Catalysis, 2016, 7, 912-918.
14. Y. Okamoto, T. Kubota, H. Gotoh, Y. Ohto, H. Aritani, T. Tanaka and S. Yoshida, Journal of the Chemical Society, Faraday Transactions, 1998, 94, 3743-3752.
15. B. Yan, S. Yao, S. Kattel, Q. Wu, Z. Xie, E. Gomez, P. Liu, D. Su and J. G. Chen, Proceedings of the National Academy of Sciences of the United States of America, 2018, 115, 8278-8283.
16. A. Figueroba, G. Kovács, A. Bruix and K. M. Neyman, Catalysis Science & Technology, 2016, 6, 6806-6813.
17. Z. Zhang, D. Han, S. Wei and Y. Zhang, Journal of Catalysis, 2010, 276, 16-23.
18. E. van Steen and F. F. Prinsloo, Catalysis Today, 2002, 71, 327-334.
19. L.-h. Xiao, K.-p. Sun, X.-l. Xu and X.-n. Li, Catalysis Communications, 2005, 6, 796-801.
20. J. Serrano-Ruiz, A. Sepúlveda-Escribano and F. Rodríguez-Reinoso, Journal of Catalysis, 2007, 246, 158-165.
21. L. Lin, S. Yao, Z. Liu, F. Zhang, L. Na, D. Vovchok, A. Martinez-Arias, R. Castaneda, J. Y. Lin and S. D. Senanayake, The Journal of Physical Chemistry C, 2018.
22. F. Zhang, Z. Liu, S. Zhang, N. Akter, R. M. Palomino, D. Vovchok, I. Orozco, D. Salazar, J. A. Rodriguez and J. Llorca, ACS catalysis, 2018, 8, 3550-3560.
23. S. Y. Yao, W. Q. Xu, A. C. Johnston-Peck, F. Z. Zhao, Z. Y. Liu, S. Luo, S. D. Senanayake, A. Martinez-Arias, W. J. Liu and J. A. Rodriguez, Physical chemistry chemical physics : PCCP, 2014, 16, 17183-17195.
24. J. F. Moulder, W. F. Stickle, P. E. Sobol and K. D. Bomben, Google Scholar, 2000, 261.
25. L. E. D. C. D. Wagner, M. V. Zeller, J. A. Taylor, R. H. Raymond, L. H. Gale, Surface and Interface Analysis, 1981, 3, 211-225.
26. S. Yao, B. Yan, Z. Jiang, Z. Liu, Q. Wu, J. H. Lee and J. G. Chen, ACS Catalysis, 2018, 8, 5374-5381.
27. B. Ravel and M. Newville, Journal of synchrotron radiation, 2005, 12, 537-541.
28. W.-W. Wang, W.-Z. Yu, P.-P. Du, H. Xu, Z. Jin, R. Si, C. Ma, S. Shi, C.-J. Jia and C.-H. Yan, ACS Catalysis, 2017, 7, 1313-1329.
29. S. Kameoka, T. Tanabe and A. P. Tsai, Catalysis Letters, 2005, 100, 89-93.
30. M. Meledina, S. Turner, V. Galvita, H. Poelman, G. Marin and G. Van Tendeloo, Nanoscale, 2015, 7, 3196-3204.
31. A. Navrotsky, C. Ma, K. Lilova and N. Birkner, science, 2010, 330, 199-201.
32. S. Hayun, S. V. Ushakov and A. Navrotsky, Journal of the American Ceramic Society, 2011, 94, 3679-3682.
33. J. Kondo, Chemical communications, 1998, 357-358.
34. Y. Wang, F. Wang, Y. Chen, D. Zhang, B. Li, S. Kang, X. Li and L. Cui, Applied Catalysis B: Environmental, 2014, 147, 602-609.
35. A. M. Beale and B. M. Weckhuysen, Physical chemistry chemical physics : PCCP, 2010, 12, 5562-5574.
36. C. T. Campbell and C. H. Peden, Science, 2005, 309, 713-714.
37. T.R. Reina, S. Ivanova, M.I. Dominguez, M.A. Centeno and J.A. Odriozola, Applied Catal. A: General, 2012, 419-420, 58-66.
38. T.R. Reina, W. Xu, M.A. Centeno, J. Hanson, J.A. Rodriguez, and J.A. Odriozola, Catal. Today, 2013, 205, 41-48.
39. T.R. Reina, S. Ivanova, V. Idakiev, J.J. Delgado, I. Ivanov, T. Tbakova, M.A. Centeno and J.A. Odriozola, Catal. Sci. Technol. 2013, 3, 779-787.

TOC

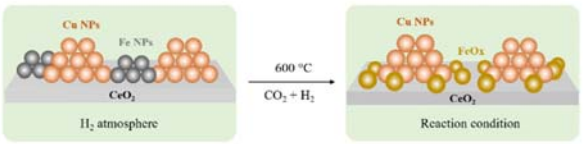

TOC

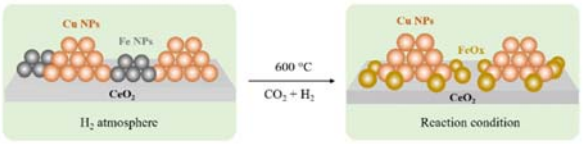


Oxide-oxide interactions have been used to control textural properties and produce active and stable $Cu/FeO_x/CeO_2$ catalysts